J. Webster (ed.), *Wiley Encyclopedia of Electrical and Electronics Engineering*

DISTRIBUTED BRAGG REFLECTOR LASERS

One of the distinguishing characteristics of a laser, as opposed to other sources of light, is that its emission consists very nearly of a single frequency, or color, of light. However, close inspection of the light emitted from a simple semiconductor laser source reveals that its light output consists of several closely spaced frequencies, and thus its spectrum is not infinitely narrow. The characteristic of single-frequency emission is critical for some applications, including optical communications and spectroscopy. One method of narrowing the emission spectrum of a simple semiconductor laser source is to incorporate in the laser a structure that is capable of selectively reflecting only one frequency of light. A distributed Bragg reflector (*DBR*) is just such a structure. Semiconductor lasers that have *DBR*s incorporated in them have single-frequency output. Emission spectra from two semiconductor lasers, one with and one without a *DBR*, are shown in Fig. 1. While other single-frequency laser sources exist, semiconductor *DBR* lasers are preferred for many applications because they are relatively simple, compact, and robust and operate over a large temperature and current range, whereas alternative sources may be complex and bulky and require precise alignment.

The use of a *DBR* to make a single-frequency laser source is only one of the several ways that a *DBR* can be used to improve or otherwise make possible certain operating characteristics of a semiconductor laser. This article describes the basic operating principles of a *DBR* and specifically how it is implemented in two types of semiconductor lasers: edge-emitting lasers and vertical cavity surface-emitting lasers. Design and fabrication issues for both types of laser are presented, as well as some of the advantages afforded by each design.

Dbr and Laser Basics

The DBR Concept. When light crosses a boundary between two materials that have different indices of refraction, n_i, the light experiences a partial reflection given by

$$r = \frac{n_1 - n_2}{n_1 + n_2} \tag{1}$$

A *DBR* is a structure that has a change in its refractive index that is repeated several times in a set period, termed the Bragg period, Λ. The periodic change in the refractive index causes multiple partial reflections that add constructively to create a strong reflection. Figure 2 is a simplified picture of how these multiple partial reflections can add to form a strong reflection. As will be shown later, this type of additive reflection is maximized when the incident light has a wave-length that is equal to twice the period of the Bragg reflector, Λ. A *DBR* is useful in two respects: it can create a strong reflection, and the reflection created is wavelength specific, that is, it reflects some frequencies of light while allowing other frequencies of light to pass through unreflected.

The Semiconductor Laser. Before developing further how a *DBR* can be used to improve a laser's performance, it is important to have clear understanding of the fundamentals of laser operation. Three factors are required for laser operation: an amplifying or gain medium, a resonant cavity for feedback, and some means

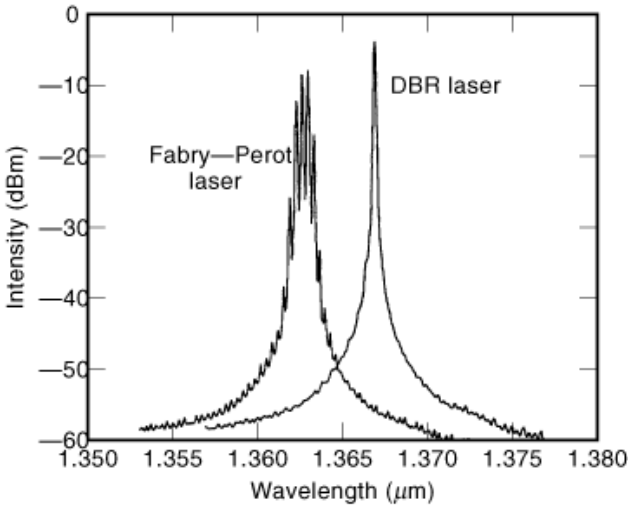

Fig. 1. Optical spectra of InGaAsP–InP ridge-waveguide lasers. Several longitudinal modes exist in the simple Fabry–Perot laser, whereas the *DBR* laser exhibits single-frequency operation.

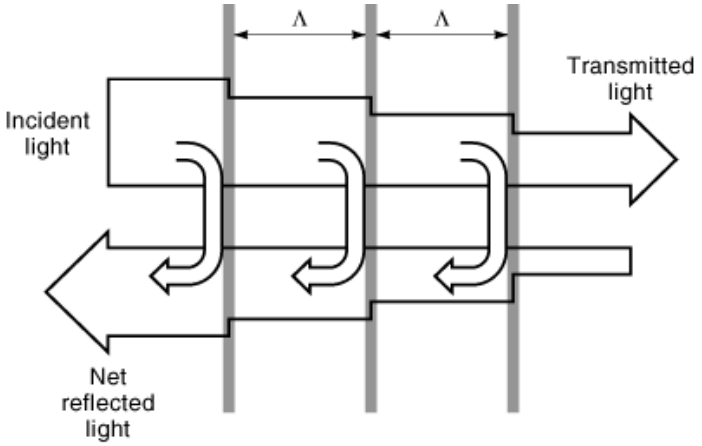

Fig. 2. Simplified pictorial of how multiple partial reflections can add to create a strong effective reflection in a *DBR* with a period λ.

of excitation. In a semiconductor diode laser, recombination of electrons and holes in the diode junction results in light emission, and a population inversion of these carriers provides optical gain. The resonant cavity for a semiconductor laser is formed by an optical waveguide with partially transparent mirrors on either end. An electric current flowing through the diode is the source of excitation. The onset of lasing action occurs when the excited gain medium begins to create just enough light to offset the loss of light due to internal losses within the cavity and the loss of light through the semitransparent mirrors. This condition is given by the equation

$$\alpha_{\text{int}} L + \frac{1}{2} \ln\left(\frac{1}{R_1 R_2}\right) = gL \qquad (2)$$

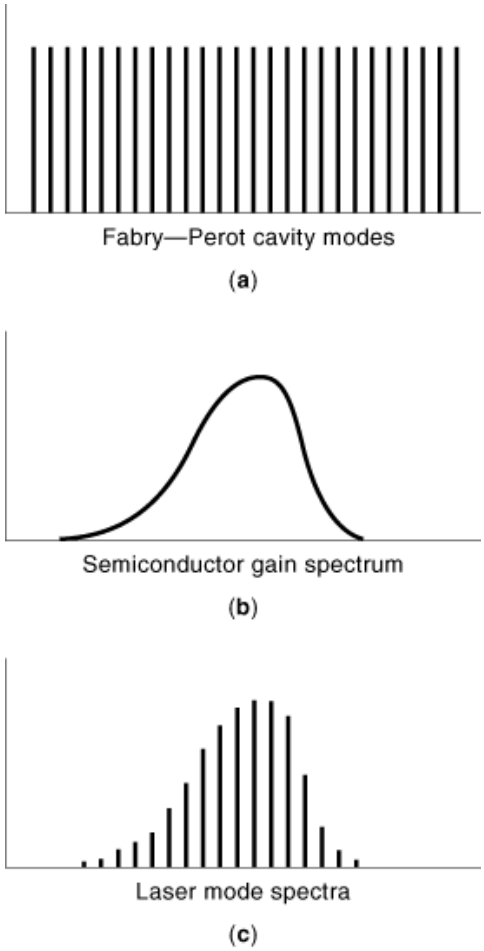

Fig. 3. A schematic diagram of (a) wavelengths at which Fabry–Perot modes exist, (b) the gain distribution in a semiconductor laser, and (c) the superposition of (a) and (b) showing the possible laser modes in a simple Fabry–Perot laser. All three graphs are plots as a function of wavelength.

where α_{int} is the internal loss, g is the gain, L is the length of the cavity, and R_1 and R_2 are power reflectivities of the two semitransparent mirrors.

The frequency of the laser light is governed by the energy distribution the gain medium is capable of providing and by the geometry of the resonant cavity. The cavity constrains the emission to discrete frequencies of light, or Fabry–Perot modes, whose half-wavelengths will fit in the cavity an integral number of times. The smaller the cavity, the greater the spacing between adjacent Fabry–Perot modes. Because the round-trip cavity loss is fairly constant for different modes, the laser emission from a simple semiconductor diode laser, usually called a Fabry–Perot laser, will consist of multiple Fabry–Perot modes that coincide with the highest gain of the material (see Fig. 3).

Edge-Emitting Lasers. Simple edge-emitting semiconductor lasers are formed by first growing a planar optical waveguide and diode junction by a suitable epitaxial growth technique. The laser is completed when the semiconductor is cleaved in two places to produce reflective facets that terminate the planar waveguide. Laser light propagates in the plane of the semiconductor wafer and is emitted from the facet formed by the

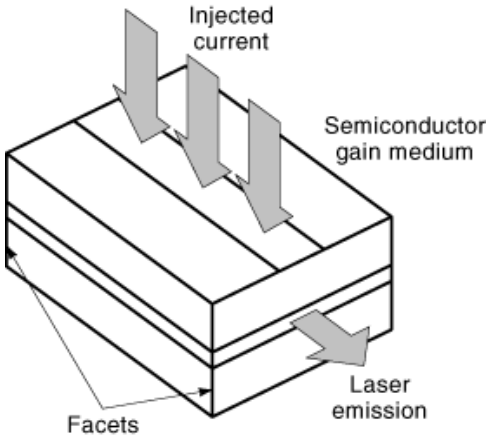

Fig. 4. A schematic diagram of a simple Fabry–Perot semiconductor diode laser. Laser light propagates in the plane of the semiconductor wafer and is emitted from the facet formed by the cleave at the edge of the wafer.

cleave at the edge of the wafer. Figure 4 shows a diagram of a simple Fabry–Perot edge-emitting laser fabricated in this fashion.The facets formed by the cleave reflect due to the change in the index of refraction between the semiconductor ($n \sim 3.5$) and the air ($n \sim 1$). The simple mirrors formed by the cleave reflect almost all frequencies of light equally well, and hence many frequencies can and do experience enough reflective feedback to lase. By replacing one or both of the facet reflectors with *DBR*s, the feedback created by the reflection can be made wavelength selective. Thus, only the frequency of light that experiences a strong reflection from the *DBR* will have enough feedback to lase. The *DBR*s are formed by etching a grating in the semiconductor. The area where material is removed from the etched portion of the grating will have an index of refraction different from that of the unetched material, creating a periodicariation in the refractive index.

Vertical Cavity Surface-Emitting Lasers. Advances in epitaxial growth techniques have recently made possible an alternative laser design that promise to provide several advantages over the more traditional edge-emitter laser. The geometry of the vertical cavity surface-emitting laser (*VCSEL*) is rotated 90° from that of the edge-emitter, and light emits from the surface of the wafer, rather than from the edge (see Fig. 5). The feedback mirrors are formed by epitaxially grown *DBR*s, which consist of alternating layers of two materials with different refractive indices. This method of creating a periodic change in refractive index is clearly different from the etched grating utilized in edge-emitting lasers. The reason *DBR*s are used in each of the lasers is also different. In edge-emitting *DBR* lasers, the grating provides a wavelength-selective mirror, which is useful because it constrains the laser to operate at a single frequency. *VCSEL*s, on the other hand, operate at a single frequency because theresonant cavity is very short, usually only one wavelength long. While the short cavity creates a single-mode operation, it also causes the gain path to be very short. Consequently, the mirror reflectivies must be very high in order to satisfy the requirements for lasing. In *VCSEL*s, the *DBR*s are used to obtain a mirrors with extremely high reflectivities.

The Bragg Period

A simplified model of wavelength-selective reflection can give insight into how a *DBR* works. Consider a strong electromagnetic wave, which can be represented by the real part of $E_0\, e^{-jkz}$, incident upon a structure of period Λ at $z = 0$ (see Fig. 6). Assume only a negligibly small part, $\Delta\rho$ of the incident wave is reflected back at each

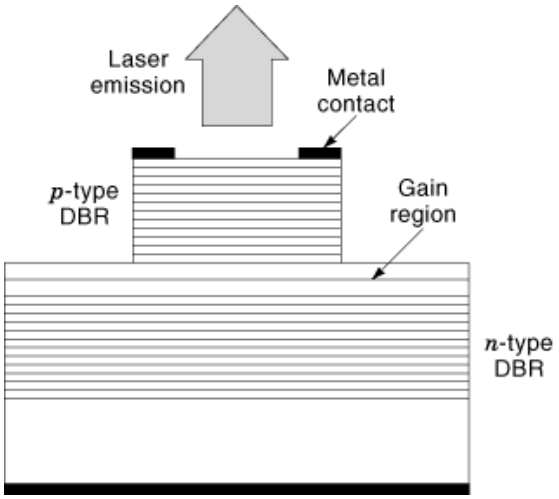

Fig. 5. A schematic diagram of a *VCSEL*. The geometry of the *VCSEL* is rotated 90° from that of the edge emitter, and light emits from the surface of the wafer. The feedback mirrors are epitaxially grown *DBR*s.

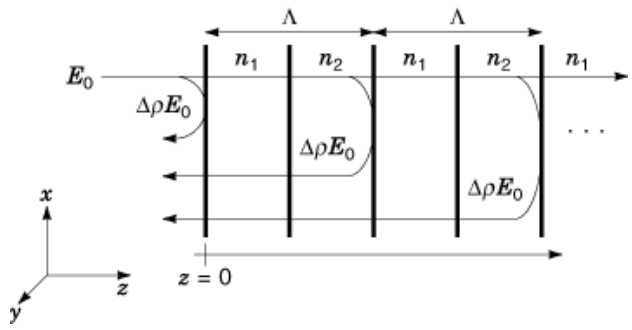

Fig. 6. A schematic diagram of light incident on a structure with a periodic refraction index. In order for the small reflections to interfere constructively and provide a large effective reflection, the periodic structure must satisfy the Bragg condition, $\Lambda = m\lambda/2$.

interface. The reflected wave at $z = 0$ can be expressed as the sum of the small reflections at each of the interfaces

$$E_{-}(z=0) = \Delta\rho E_0 e^{(-j0)} + \Delta\rho E_0 e^{(-jk2\Lambda)} + \Delta\rho E_0 e^{(-jk4\Lambda)} + \cdots \quad (3)$$

Note that the phase components of the individual reflected waves are integer multiples of $2k\Lambda$, where k is the wave number $(2\pi/\lambda)$ of the propagating wave. For these small reflections to constructively interfere (sum) and provide a large effective reflection, $2k\Lambda$ must equal an integer multiple of 2π radians. This model is not strictly valid because we have ignored the fact that the magnitude of the incident wave, E_0, decreases and that the backward traveling reflections will be partially reflected in the forward direction again. Nevertheless, the model leads to an important concept: a periodic structure can provide a wavelength-selective reflection when

the period, Λ is equal to an integer multiple of half wavelengths

$$2k\Lambda = 2m\pi \tag{4}$$

$$\Lambda = \frac{m\lambda}{2} \tag{5}$$

where we have used the fact that $k = 2\pi/\lambda$ and defined $\lambda = \lambda_0/n_0$. The parameters λ_0 and n_0 are, respectively, the free-space wavelength and the effective index of the laser mode. The order of the grating is designated by the integer m.

Edge-Emitting Single Frequency Lasers

Both distributed feedback (*DFB*) lasers and *DBR* lasers utilize Bragg reflectors to induce single-frequency operation. The distinction between *DFB* lasers and *DBR* lasers lies in the placement of the Bragg grating (see Fig. 7). In a *DFB* laser, the grating that provides distributed feedback is placed along the entire length of the laser, whereas in the *DBR* laser, the grating does not overlap the active region, and is used only at the end of the cavity as a wavelength-selective mirror. In 1972, Kogelnik and Shank outlined the principles behind the operation of *DFB* lasers using a coupled wave model (1). Coupled-mode theory explains the operation of both *DBR* and *DFB* lasers; however, the lasers realize single-frequency operation by two distinctly different methods. In a *DFB* laser, only modes that can propagate in the periodic structure will exist. Of the allowed modes, the mode nearest the Bragg wavelength will lase. In a *DBR* laser, where the Bragg grating is used as a reflector, modes that can propagate through the periodic structure will not experience any feedback and therefore cannot resonate and will not lase. The cavity mode that experiences the strongest reflection from the *DBR* will lase, assuming the mode overlaps the gain spectrum of the material. *DFB* lasers were demonstrated in 1974 (1), and demonstration of *DBR* lasers followed in 1975 (2).

Coupled-Mode Theory.

Coupling Coefficient. To create a high degree of wavelength selectivity, the periodic structure must satisfy the Bragg condition, and it must effectively interact with the optical mode in the laser structure. Within a laser cavity, there are both forward- and backward-propagating waves. These waves are "coupled" through the distributed reflections within the periodic structure. The coupling coefficient κ describes the degree of interaction between the forward- and backward-propagating waves.

The coupling coefficient can be determined by applying coupled-mode theory. Let us start with a periodically varying index of refraction profile and use the coordinate system defined in Fig. 6

$$n(z) = n_0 + \Delta n \cos(2\beta_0 z), \qquad \Delta n \ll n_0 \tag{6}$$

Note that any index variation profile, $n(z)$, can be expressed in a similar expression by the Fourier expansion of the function that describes the index variation. By making the approximation that the variations of the optical field in the x and y directions are negligible, the wave equation for the optical field along the laser cavity (z direction) can be written as

$$\frac{\partial^2 E(z)}{\partial z^2} + n^2(z)k^2 E(z) = 0 \tag{7}$$

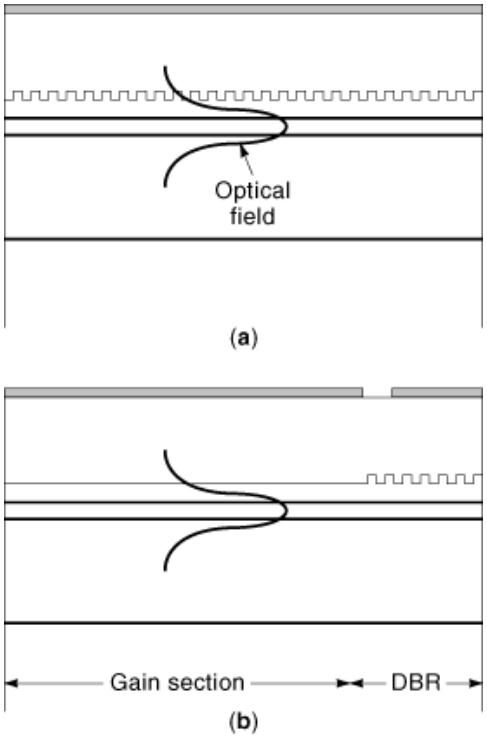

Fig. 7. Schematic diagrams of a (a) *DFB* laser and (b) *DBR* laser, with a diagram of the optical field intensity inside the laser superimposed. The feedback mechanism (grating) is distributed along the entire length of the cavity in a *DFB* laser, but is separated from the gain section in for *DBR* laser.

When $n(z)$ is squared, the term including $(\Delta n)^2$ can be neglected. Therefore

$$n^2(z) = [n_0 + \Delta n \cos(2\beta_0 z)]^2 \approx n_0^2 + 2\Delta n(n_0)\cos(2\beta_0 z) \quad (8)$$

$$\begin{aligned} k^2 n^2(z) &= \left(\frac{2\pi}{\lambda}\right)^2 \left(n_0^2 + 2\Delta n(n_0)\cos(2\beta_0 z)\right) \\ &= \beta^2 + 4\beta\kappa \cos(2\beta_0 z) \end{aligned} \quad (9)$$

where $\beta = (2\pi/\lambda)n_0$ and $\kappa = (\pi/\lambda)\Delta n$.

The complex propagation constant β is assumed to be very close to the Bragg propagation constant β_0.

$$\beta = (\beta_0 + \delta) + j\alpha_0 \qquad (\delta, \alpha_0 \ll \beta_0) \quad (10)$$

where δ is the detuning parameter that represents the separation of β from the Bragg propagation constant, and α_0 represents the gain or loss in the medium.

Next, we assume that the solution for the field, $E(z)$, can be written as the superposition of a forward- and backward-propagating components, with propagation constant β_0.

$$E(z) = A(z)\exp(-j\beta_0 z) + B(z)\exp(+j\beta_0 z) \qquad (11)$$

The assumptions of Eq. (10) will result in $A(z)$ and $B(z)$ being slowly varying functions of z.

Equations (9) and (11) can then be substituted into Eq. (7). The first term of Eq. (7) becomes

$$\frac{\partial^2 E(z)}{\partial z^2} = \frac{\partial^2}{\partial z^2}[A(z)\exp(-j\beta_0 z) + B(z)\exp(+j\beta_0 z)] \qquad (12)$$

The second derivative terms, d^2A/dz^2 and d^2B/dz^2, can be neglected because, as mentioned before, A and B are slowly varying functions

$$\begin{aligned}\frac{\partial^2 E(z)}{\partial z^2} \approx & -2j\beta_0 \frac{dA(z)}{\mathrm{d}z}\exp(-j\beta_0 z) - (\beta_0)^2 A(z)\exp(-j\beta_0 z) \\ & +2j\beta_0 \frac{dB(z)}{dz}\exp(+j\beta_0 z) \\ & -(\beta_0)^2 B(z)\exp(+j\beta_0 z)\end{aligned} \qquad (13)$$

The second term of Eq. (7) becomes

$$\begin{aligned}k^2 n^2 E(z) &= [\beta^2 + 4\beta\kappa\ \cos(2\beta_0 z)][A(z)\exp(-j\beta_0 z) + B(z)\exp(+j\beta_0 z)] \\ &\approx \beta^2[A(z)\exp(-j\beta_0 z) + B(z)\exp(+j\beta_0 z)] \\ &\quad +2\beta\kappa[A(z)\exp(+j\beta_0 z) + B(z)\exp(-j\beta_0 z)]\end{aligned} \qquad (14)$$

where the Euler identity has been used and third-harmonic terms have been neglected.

Collecting terms with common phase components and utilizing the assumption that $\beta \gg \alpha,\delta$ result in the coupled-mode equations

$$\frac{dA(z)}{dz} = (\alpha_0 - j\delta)A(z) - j\kappa B(z) \qquad (15)$$

$$\frac{dB(z)}{dz} = -(\alpha_0 - j\delta)B(z) + j\kappa A(z) \qquad (16)$$

These equations show that the forward-propagating term $A(z)$ is coupled to the backward-propagating term, $B(z)$, by κ, and vice versa.

Thus far, the periodic index variation has been assumed to be infinite in the x and y directions. However, in a laser structure,the gratings (the periodic structure) have a finite dimension. Therefore, only a portion of the optical mode overlaps the periodic index variation. The expression for the coupling coefficient now must account for the spatial extent (x direction) of the index variation

$$\kappa = \frac{\omega}{4}\int_{-\infty}^{\infty} d(x)|E(x)|^2\,dx \qquad (17)$$

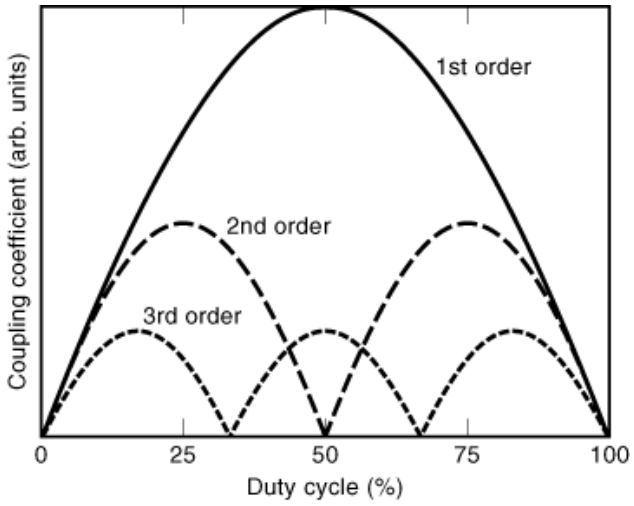

Fig. 8. Schematic diagram of the coupling coefficient κ, as a function of grating duty cycle for three different ordered gratings. The coupling coefficient is larger for lower order gratings. For odd-order gratings, there is maximum coupling at 50% duty cycle. For even-order gratings, a null exists at 50%.

Here, $d(x)$ is the Fourier expansion of the periodic index variation. Therefore, to obtain a large coupling coefficient κ, the optical mode and the periodic structure should overlap strongly [large $E(x)$], or the index variation $d(x)$ should be sufficiently large.

Depending on the order of the grating, different duty cycles are required to achieve maximum coupling. A duty cycle is the length of the high-index region within the period devided by the period. Figure 8 shows a schematic diagram of how the coupling varies with the duty cycle. For odd-order gratings, there is maximum coupling at 50% duty cycle. For even-order gratings, a null exists at 50% duty cycle. The coupling coefficient is larger for lower-order gratings.

In summary, several factors must be considered to achieve the desired coupling coefficient: the placement of the gratings within the laser structure, the order of the gratings, and the duty cycle are all factors that affect the coupling coefficient.

Reflectivity. The reflectivity of a periodic structure is determined from the coupled-mode equations. Note that the coupled-mode equations are linear, first-order differential equations. Therefore, the general solutions to the coupled-mode equations have the form of

$$A(z) = A_+\exp(+\gamma z) + A_-\exp(-\gamma z) \qquad (18)$$

$$B(z) = B_+\exp(+\gamma z) + B_-\exp(-\gamma z) \qquad (19)$$

Substituting Eqs. (18) and (19) into Eqs. (15) and (16), the coupled-mode equations, yields

$$\begin{bmatrix} \gamma - (\alpha_0 - j\delta) & +j\kappa \\ j\kappa & -\gamma - (\alpha_0 - j\delta) \end{bmatrix} \begin{bmatrix} A_+ \\ B_+ \end{bmatrix} = 0 \qquad (20)$$

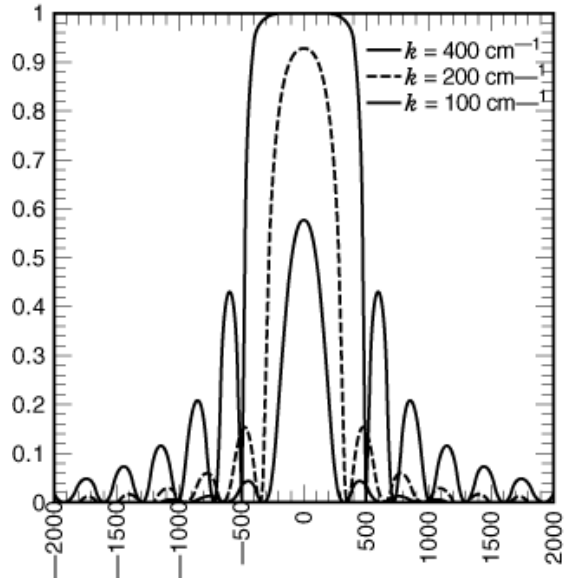

Fig. 9. Reflectivity of lossless ($\alpha_0 = 0$) *DBR* gratings for $L = 100$ μm with $\kappa = 100$ cm^{-1} and $\kappa = 400$ cm^{-1}. Note that larger κ yields a higher reflectivity and a wider stop band.

$$\begin{bmatrix} -\gamma - (\alpha_0 - j\delta) & +j\kappa \\ j\kappa & \gamma - (\alpha_0 - j\delta) \end{bmatrix} \begin{bmatrix} A_- \\ B_- \end{bmatrix} = 0 \qquad (21)$$

In order for these equations to result in a nontrivial solution, the determinants of both matrices must equal to zero. Making this assignment yields

$$\gamma^2 = \kappa^2 + (\alpha_0 - j\delta)^2 \qquad (22)$$

Now, consider a periodic structure of length L with a forward traveling wave incident on it. For simplicity, assume that the strength of the incident wave, $A(z = 0)$, is known, the structure is lossless ($\alpha_0 = 0$), and the backward traveling wave is zero at L, $B(z = L)$. These boundary conditions reduce Eqs. (18) and (19) to a system of two equations and two unknowns. Using Eq. (22), it is possible to derive expressions for $A(z)$ and $B(z)$ in terms of $A(z = 0)$. The reflectivity at $z = 0$ is then expressed as a ratio between the backward- and forward-propagating components:

$$r(0) = \frac{B(0)}{A(0)} = \frac{-j\kappa \sinh(\gamma L)}{\gamma \cosh(\gamma L) - (\alpha_0 - j\delta)\sinh(\gamma L)} \qquad (23)$$

A plot of $|r(0)|^2$ versus δ, the detuning parameter, for two different values of κ is shown in Fig. 9. The region of high reflection near $\delta = 0$ is called the *stop band*. The plot clearly shows that the reflectivity and the width of the stop band increases with increasing κ. The reflectivity also increases with the length of the grating, L.

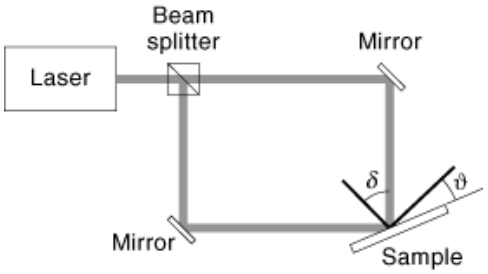

Fig. 10. A schematic diagram of a holographic interference lithography setup. An interference pattern is formed when the two beams are brought together on the surface of the sample. The interference pattern is photolithographically transferred to the sample, which is spin-coated with photoresist.

Grating Fabrication. In 1975, Reinhart et al. used holographic interference and ion milling to create a third-order *DBR* grating. Since then, the fabricationand epitaxial technologies have improved steadily, and these advances allow the design and fabrication of more sophisticated and complex devices.

The small dimensions of the gratings, on the order of a few hundred nanometers, preclude the use of conventional photolithography for their fabrication. Although recent advance have greatly reduced the minimum feature size attainable by photolithography, two other methods are more common for gratings fabrication today: holographic interference and direct-write electron-beam lithography.

A typical setup for holographic interference is shown in Fig. 10. The output of a laser is split into two beams that are expanded and collimated. An interference pattern is formed when the two beams are brought together on the surface of the sample. The interference pattern is photolithographically transferred to the sample, which is spin-coated with photoresist. By choosing a laser with the proper laser wavelength (λ) and controlling the angles of the sample and beam incidence (ϑ and δ), it is possible to fabricate gratings with different periods (pitches)

$$\Lambda = \frac{\lambda}{2 \sin \delta \cos \vartheta} \tag{24}$$

This simple technique has been used since the first fabrication of *DBR* lasers. Because of its high throughput, the holographic interference method is the most common fabrication technique used to produce *DBR* and *DFB* lasers commercially. More complicated exposure schemes using multiple resist and phase shifting, among others can be used to create gratings with more complex characteristics.

Electron-beam direct-write lithography is an alternative method for fabricating gratings. An electron beam is used to write gratings on a sample spin-coated with a resist, typically polymethylmethacrylate (*PMMA*). The accuracy of the period and duty cycle of the grating generated by electron beam direct-write lithography depends on several factors, including the electron-beam current, the electron-beam size, and the scanning system. Although electron-beam direct-write lithography has been used togenerate gratings for high-performance lasers, slow writing speed and high system cost limit its application in the commercial sector.

Once gratings have been lithographically transferred into a resist, the next step is to etch the grating pattern into the underlying semiconductor.Wet etching is a simple and easy process that causes little damage to the semiconductor crystal. Precise etch depths can be achieved by utilizing selective wet etches. Lateral dimensions can be much more precisely controlled by using dryetching techniques rather than using a wet etch. However, dry etching can cause crystal damage that may need to be repaired before further processing.

The location of the gratings in the laser structure and the material system of the epitaxial layers determine the subsequent processing. Typically,gratings are placed near the active region of the laser structure, where the optical mode is strongest. Locating the grating near the peak of the optical mode creates strong coupling, but it requires that the epitaxial growth of the laserbe done in two steps, with the grating etch performed in between the two growths. Because the optical mode interacts strongly with the grating, large variations in the refractive index are not necessary [see Eq. (17)] and the depth of the gratings can remain small, which is desirable when regrowth is necessary. Special care must be taken to preserve the shape of the gratings during subsequent epitaxial growth because they can be deformed by mass transport. In the InP–InGaAsP material system, regrowth is fairly trouble-free when the sample is properly prepared. However, in the GaAs–AlGaAs material system, regrowth over gratings is can be problematic because of the highly reactive nature of Al-containing compounds.

To circumvent this problem, aluminum-containing laser structures areusually grown in a single step, and gratings are etched on the surface of the laser. However, the placement of the gratings on the surface reduces the amountof interaction between the optical mode and the grating because the optical mode is tightly confined within the cladding layers, and only the tail of the optical mode can interact with the grating. As seen in Eq. (17), to achieve an appreciable value for κ, a large index change in the grating structure is necessary to compensate for the small overlap of the optical mode with the grating. To create this large change in refractive index, the gratings must be etched fairly deeply (0.8 μm 1.0 μm) into the epitaxial layers. Because the grating dimensions are only a few hundred nanometers and the etch depth may be a 1 μm or more, the aspect ratio of the grating is very large. The task of etching these large-aspect-ratio features into the semiconductor while preserving the period, duty cycle, and shape is difficult to perform even with dry etching processes such as reactive ion etching (*RIE*). More sophisticated dry etching techniques such as chemically assisted ion beam etching (*CAIBE*) are often necessary to achieve the highly anisotropic etch demanded by the high-aspect-ratio grating. *DBR* lasers with a thinner upper cladding, often called asymmetric cladding lasers, can be used to circumvent this difficulty. Because the upper cladding is thinner, typically 0.3 μm to 0.4 μm, the field is stronger at the surface and adequate coupling can be achieved even with a shallow grating etch (< 0.25 μm).

Ridge waveguides, buried ridge waveguides, and buried heterostructures are some of the device configurations to provide lateral confinement, both optical and electrical, necessary for improved performance of the *DBR* laser.

Wavelength-Tunable DBR Lasers. For various applications such as wavelength-division multiplexing and light detection and ranging LIDAR spectroscopy, wavelength-tunable *DBR* lasers are highly desirable. It is possible to tune *DBR* lasers efficiently by injecting a current into the *DBR* section of the laser (3). Current injection causes the refractive index of the semiconductor to change, which in turn changes the Bragg wavelength of the grating, as seen in Eq. (5). Figure 11 shows a schematic diagram of a wavelength-tunable *DBR* laser. The contact pads of the gain section and the tuning section of the laser are isolated so that each section can be biased independently.

There are two mechanisms by which current injection changes the refractive index of a semiconductor. Injected free carriers and band-filling effects cause a decrease in the index of refraction. This phenomenon is referred to as the plasma effect and is described by

$$\Delta n = n_f - n_0 = -\frac{1}{n_0}\frac{n_e e^2}{m_e^* \epsilon_0}\frac{\lambda^2}{4\pi^2 c^2} \qquad (25)$$

where n_0 is the index of refraction, n_e is the electron concentration, and $m*_e$ is the effective electron mass.

Current injection also causes heating of the laser structure, which creates in an increase in the index of refraction. Therefore, injecting carriers to the *DBR* section can tune the output of a *DBR* laser to a longer or shorter wavelength, depending on which mechanism dominates. The plasma effect increases as a function

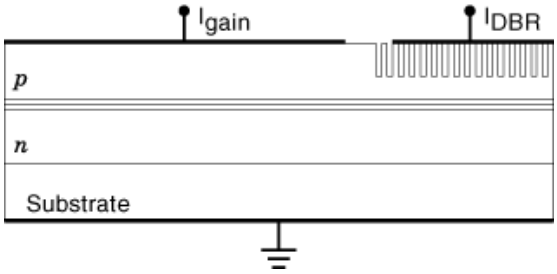

Fig. 11. Schematic diagram of a tunable *DBR* laser showing the isolated contact pads of the gain section and the tuning section of the laser so that each section can be biased independently. It is possible to tune *DBR* lasers efficiently by injecting a current into the *DBR* section of the laser.

of λ^2. Thus, in the long-wavelength InP material system, current injection into the tuning section decreases the Bragg wavelength. The heating mechanism dominates in the shorter-wavelength GaAs material system, resulting in an increase of the Bragg wavelength.

Tuning is not continuous with tuning current but is interrupted by mode hops. As the peak Bragg reflection shifts, the lasing wavelength also shifts. When the peak shifts over far enough, an adjacent cavity mode will experience a higher reflectivity. This selection of successive cavity modes causes "mode hopping" in the wavelength tuning characteristic. The addition of a third phase controlling section can extend the continuous tuning range (4). The tuning range is typically limited by the amount of index shift that can be achieved in the mirror ($\Delta\lambda/\lambda = \Delta n/n$). A maximum tuning range of ~1% of the wavelength is common (5). Increased tuning range can be achieved when more complex structures and tuning schemes such as superstructure gratings and sampled gratings are employed (6,7).

Integrated DBR lasers. Because the gratings eliminate the need for cleaved facets, and the reflectivity can be controlled by the length, depth, and order of the grating, it is possible to design and fabricate *DBR* lasers with monolithically integrated waveguides, modulators, and amplifiers. The separation of the active and grating sections of the laser enables the laser to be interconnected with other optical components using a continuous waveguide that permits high optical coupling between the source and these components. The laser structure can be optimized for improved performance with these devices by smoothly integrating regions with different bandgaps. One technique for achieving in-plane bandgap tuning within a single epitaxial growth is selective area epitaxy (*SAE*). For example, Lammert et al. have demonstrated an electroabsorption modulator integrated with a *DBR* laser utilizing SAE (8). The bandgap of the modulator section is designed to be larger than the bandgap of the laser. Therefore, the modulator is transparent until a modest reverse bias is applied to shift the absorption peak to extinguish the output signal from the *DBR* laser.

Vcsel

The concept of the *VCSEL*, a surface-emitting diode laser formed by sandwiching a *p–n* junction between two epitaxially grown *DBR* mirrors, was initially conceived by Soda et al. at the Tokyo Institute of Technology in 1979 (9). The *VCSEL*, although requiring more complex and exacting crystal-growth processes, has several advantages over the edge-emitting laser. Aside from the more complicated epitaxial growth, the *VCSEL* is a more attractive candidate for manufacturing. Because the *VCSEL* does not require etched or cleaved facets, these devices can be fully tested at the wafer level, before committing to further processing steps. It is also much smaller than an edge-emitting laser, so more devices can be produced from each wafer. The all planar processing of the *VCSEL* also facilitates integration of the *VCSEL* with other electronic devices.

The attribute of surface emission, in addition to eliminating the need for cleaved facets, makes possible the fabrication of two-dimensional arrays of lasers, which lends itself to applications in parallel communications. Or, by allowing the growth thickness to change across the wafer, each *VCSEL* in the array can be made to lase at a slightly different frequency, which allows for wavelength-division multiplexing (*WDM*).

One serious drawback of the edge-emitting laser is its highly elliptical and astigmatic beam pattern, which arises from the aspect ratio of the laser's aperture (thin and wide). Such a beam pattern requires the use of additional optics in many applications, such as coupling to an optical fiber. There is much more control over the design of the aperture and beam pattern of the *VCSEL*, and consequently the emission beam pattern has much better characteristics.

The smaller size of the *VCSEL* improves operating performance because of smaller drive currents, capacitances, and power requirements. Moreover, because the cavity of the *VCSEL* is very short, only one longitudinal mode can exist, so the emission is inherently single longitudinal mode. A drawback of the small size is that the *VCSEL* output power is small as well.

VCSEL Design. Because the gain path in a *VCSEL* is very short (twice the length of the cavity, typically 2λ), the reflectivity of the cavity mirrors must be extremely high ($>99\%$) to satisfy the requirement for lasing

$$1 \leq \Gamma_u^2 \Gamma_l^2 e^{2\alpha_0 L} \tag{26}$$

where Γ_u and Γ_l are the total field reflectivities of the upper and lower mirrors, L is the length of the cavity, and α_0 is the gain coefficient. The equation for the net reflectivity of a *VCSEL DBR* mirror is given by the formula for a plane wave experiencing multiple reflections and is found in many textbooks

$$\Gamma_{i+1}(\lambda) = \frac{r_{i+1}(\lambda) + \Gamma_i(\lambda) e^{-j2\beta_i(\lambda) l_i^{\text{eff}}}}{1 + r_{i+1}(\lambda)\Gamma_i(\lambda) e^{-j2\beta_i(\lambda) l_i^{\text{eff}}}}, \qquad \Gamma_1(\lambda) = r_1(\lambda) \tag{27}$$

$$r_i = \frac{n_i - n_{i+1}}{n_i + n_{i+1}} \tag{28}$$

Here Γ_i is the net field reflectivity at layer i, β_i is the propagation constant in layer i, l^i_{eff} is the effective thickness of layer i, and r_i is the local reflectivity between the layers i and $i+1$.

In order to make Γ large, two conditions are required: (1) a large number of quarter-wavelength-thick layers in the Bragg reflector, and (2) two materials with contrasting indices of refraction out of which to make the pairs. Because the *VCSEL* has only one longitudinal mode, which is determined by the length of the cavity, the cavity length must be grown with great precision to attain the desired wavelength. The length must be such that the resulting mode overlaps the gain spectrum and the stop band of the *DBR*.

Mirror Fabrication. The *VCSEL* is perhaps the most challenging optoelectronic structure to be created by crystal-growth techniques. While the concept for the *VCSEL* has been around for a long time, its performance had been limited largely due to the complexity of mirror fabrication.

InGaAs and AlGaAs lasers, which operate at shorter wavelengths (800 nm to 1100 nm), utilize AlAs–GaAs *DBR*s. AlAs and GaAs have large differences in their indices of refraction and are almost perfectly lattice matched, which makes them ideal for use in a *DBR*. AlAs–GaAs mirrors, as semiconductor materials, can be doped to allow current to flow directly through them to the active region of the laser. Even though the AlAs and GaAs have strongly contrasting indices of refraction, more than 20 pairs are needed in the *DBR* to obtain the necessary reflectivity. The multiple abrupt heterointerfaces in the mirror can create a significant electrical resistance, which leads to heating and higher power requirements. This effect can be reduced by compromising

to some degree on optical design. By grading the composition and heavily doping the heterointerfaces this series resistance can be reduced and overall performance of the *VCSEL* is improved (10).

Lasers based on InP-based material systems, which provide the longer wavelengths suitable for use in optical communications, lack semiconductor materials that are both lattice matched and have sufficient contrast in their indices of refraction to be good candidates for materials in a *DBR*. Without a substantial difference in refraction indices, the number of *DBR* pairs required poses problems both in the precision of the extended growth and with incurred diffraction losses. One solution has been to use dielectric materials having disparate refraction indices, such as ZnSe–CaF_2 or TiO_2–ZnO_2, in the Bragg reflector in place of semiconductors. Because of the insulating nature of these dielectrics, this technique leads to problems in making electric contacts and with heat dissipation. Another solution has been to use the same AlAs–GaAs *DBR*s that are used to make *VCSEL*s at the shorter wavelengths. While AlAs–GaAs mirrors cannot be grown directly on a material to which it is not lattice matched, such as InP, it can be grown separately and then later fusion bonded onto another material (10). Fusion bonding is a process using heat and pressure to adhere two semiconductors together.

Lateral Confinement. Another design aspect that has received a great deal of attention is the definition of the lateral dimensions of the *VCSEL*. Lateral definition of the cavity is needed both to efficiently funnel carriers to the active region and to provide confinement for the optical mode. Several techniques have been used for this process. One method is simply to etch away all the surrounding material from the *VCSEL*, leaving a so-called air post *VCSEL*. This provides strong electrical and optical confinement. A disadvantage of this technique is that the resulting morphology is nonplanar, making placement of electric contacts difficult. In a second technique, rather than etching away the surrounding material, it is rendered electrically insulating by ion bombardment. This technique has proved to be highly reliable and is currently used to produce *VCSEL*s commercially. For *VCSEL*s using AlAs–GaAs mirrors, selective oxidation is a recently developed technique that has proved most successful in creating small apertures, leading to smaller devices with lower threshold currents and higher efficiencies (11). In selective oxidation, aluminum-containing layers of the *DBR* mirror are oxidized, providing both electrical and optical confinement. Holes are etched in the perimeter of the *VCSEL*, and the *VCSEL* is placed in a steam environment at elevated temperatures. Oxidation initiates from the etched holes, creating a ring of oxide, the center of which forms the aperture of the *VCSEL*. The aperture size can be closely controlled by how much material is allowed to oxidize.

Conclusion

Both edge-emitting *DBR* lasers and *VCSEL*s are important laser sources for a variety of applications ranging from optical communications to spectroscopy. Because of their advantages over traditional Fabry–Perot semiconductor lasers, significant resources have been directed towards active research and development of both laser structures.

The single-longitudinal-mode operation of *DBR* lasers is a major advantage over Fabry–Perot lasers. In addition, because the cavity is defined by gratings rather than a cleave, *DBR* lasers can be monolithically integrated with other optoelectronic components. The ability to tune the output wavelengths by current injection makes *DBR* lasers excellent candidates for wavelength-division multiplexing (*WDM*) applications.

Compatibility with current integrated-circuit fabrication technologies, the possibility of two-dimensional array configurations, and on-wafer testing enable inexpensive fabrication and packaging of *VCSEL*s. As *VCSEL* technology matures, the numerous advantages of the *VCSEL* design will undoubtedly allow it to displace light-emitting diodes and edge-emitting lasers in some extisting applications as well as to foster new applications.

BIBLIOGRAPHY

1. H. Kogelnik C. V. Shank, Coupled-wave theory of distributed feedback 011lasers, *J. Appl. Phys.*, **43**: 2327–2335, 1972.
2. F. K. Reinhart, R. A. Logan, C. V. Shank, GaAs–Al_xGa_{1-x} As injection lasers with distributed Bragg reflectors, *Appl. Phys. Lett.*, **27**: 45–48, 1975.
3. S Murata, I. Mito, K. Kobayashi, Spectral characteristics for a 1.5 μm *DBR* laser with frequency-tuning region, *IEEE J. Quantum Electron.*, **QE-23**: 835–838, 1987.
4. S Murata, I. Mito, K. Kobayashi, Over 720 GHz (5.8 nm) frequency tuning by a 1.5 μm *DBR* laser with phase and Bragg wavelength control region, *Electron. Lett.*, **23**: 403–405, 1987.
5. Y. Kotaki H. Ishikawa, Wavelength tunable *DFB* and *DBR* lasers for coherent optical fibre communications, *IEE Proc.-J*, **138**: 171–177, 1991.
6. Y. Tohmori,, *et al.* Broad-range wavelength tuning in *DBR* lasers with super structure grating (*SSG*), *IEEE Photon. Technol. Lett.*, **5**: 126–129, 1993.
7. V. Jayaraman,, *et al.* Extended tuning range in sampled grating *DBR* lasers, *IEEE Photon. Technol. Lett.*, **5**: 489–491, 1993.
8. R. M. Lammert,, *et al.* MQW wavelength-tunable *DBR* lasers with monolithically integrated external cavity electroabsorption modulators with low-driving voltages fabricated by selective-area MOCVD, *IEEE Photon. Technol. Lett.*, **8**: 797–799, 1996.
9. H. Soda,, *et al.* GaInAsP/InP surface emitting injection lasers, *Jpn. J. Appl. Phys.*, **18**: 2329–2230, 1979.
10. Y. Ohiso, et al. T. Kurokawa, Long-wavelength (1.55-um) vertical-cavity lasers with InGaAsP/InP-GaAs/AlAs *DBR*s by wafer fusion, *IEEE J. Quantum Electron.*, **34**: 19047–11913, 1998.
11. W. W. Chow,, *et al.* Design, fabrication, and performance of infrared and visible vertical-cavity surface-emitting lasers, *IEEE J. Quantum Electron.*, **33**: 1810–1824, 1997.

READING LIST

G. P. Agrawal (ed.), *Semiconductor Lasers: Past, Present, and Future*, Woodbury, NY: American Institute of Physics, 1995.

J. Buus, *Single Frequency Semiconductor Lasers*, Bellingham, WA: SPIE Optical Engineering Press, 1991.

H. Casey M. Panish, *Heterostructure Lasers*, New York: Academic, 1978.

K. D. Choquette, Vertical-cavity surface emitting lasers: moving from research to manufacturing, *Proc. IEEE*, **85**: 1730–1739, 1997.

L. A. Coldren S. W. Corzine, *Diode Lasers and Photonic Integrated Circuits*, New York: Wiley, 1995.

K. S. Giboney, L. B. Aronson, B. E. Lemoff, The ideal light source for datanets, *IEEE Spectrum*, **35**: 43–53, February 1998.

T. L. Koch U. Koren, Semiconductor photonic integrated circuits, *IEEE J. Quantum Electron*, **27**: 641–653, 1991.

S. D. ROH
R. B. SWINT
J. J. COLEMAN
University of Illinois